Improving Strain-localized GaSe Single Photon Emitters with Electrical Doping

Weijun Luo, ¹ Alexander Puretzky, ^{2*} Benjamin Lawrie, ^{2,3*} Qishuo Tan, ¹ Hongze Gao, ¹ Anna K Swan, ^{4,5,6} Liangbo Liang, ² Xi Ling^{1,5,6*}

¹ Department of Chemistry, Boston University, Boston, MA 02215, United States

²Center for Nanophase Materials Sciences, Oak Ridge National Laboratory, Oak Ridge, TN 37831, United States

³ Materials Science and Technology Division, Oak Ridge National Laboratory, Oak Ridge, TN 37831, United States

⁴ Department of Electrical Engineering, Boston University, Boston, MA 02215, United States

⁵ The Photonics Center, Boston University, Boston, MA 02215, United States

⁶ Division of Materials Science and Engineering, Boston University, Boston, MA 02215, United States

*Correspondence: xiling@bu.edu; puretzkya@ornl.gov; lawriebj@ornl.gov

This manuscript has been authored in part by UT-Battelle, LLC, under contract DE-AC05-00OR22725 with the US Department of Energy (DOE). The US government retains and the publisher, by accepting the article for publication, acknowledges that the US government retains a nonexclusive, paid-up, irrevocable, worldwide license to publish or reproduce the published form of this manuscript, or allow others to do so, for US government purposes. DOE will provide public access to these results of federally sponsored research in accordance with the DOE Public Access Plan (http://energy.gov/downloads/doe-public-access-plan).

ABSTRACT

Exciton localization through nanoscale strain has been used to create highly efficient single-photon

emitters (SPEs) in 2D materials. However, the strong Coulomb interactions between excitons can

lead to non-radiative recombination through exciton-exciton annihilation, negatively impacting

SPE performance. Here, we investigate the effect of Coulomb interactions on the brightness, single

photon purity, and operating temperatures of strain-localized GaSe SPEs using electrostatic

doping. By gating GaSe to the charge neutrality point, the exciton-exciton annihilation non-

radiative pathway is suppressed, leading to ~60% improvement of emission intensity and a

reduction of the single photon purity $g^{(2)}(0)$ from 0.55 to 0.28. The operating temperature also

increases to 85 K consequently. This research provides insight into many-body interactions in

excitons confined by nanoscale strain and lays the groundwork for the optimization of SPEs for

optoelectronics and quantum photonics.

KEYWORDS: single photon emission, two-dimensional materials, gallium selenide, strain

engineering, fermi level, electrostatic doping

2

Strain-localized excitons in 2D semiconductors often exhibit single photon emission (SPE) property which is critical to the development of quantum information technologies such as quantum communication, computing, and sensing^{1–3}. While hexagonal boron nitride (hBN) and WSe₂ are two most widely studied 2D SPE hosts^{4–7}, interests in exploring the potential of other 2D materials for SPE and developing strategies to improve the SPE performance are growing in recent years^{8–10}. Particularly, Luo et al. demonstrated deterministic localization of SPEs in multilayer GaSe using nanopillar arrays¹¹, and showed that strain plays a critical role in controlling the brightness and emission wavelength of the SPE using nanoscale spatial resolution imaging technique¹². Nevertheless, significant performance improvement is still needed to satisfy the application requirements.

Previous studies have demonstrated that cavity interactions^{3,10}, defect engineering¹¹, and electrostatic doping^{12,13} can enhance the performance of SPEs in 2D semiconductors such as hBN and WSe₂. Notably, electrostatic doping has been considered as an effective and practical approach to effectively enhance the brightness, single photon purity, and operating temperatures of SPEs in monolayer WSe₂¹³ by controlling carrier concentrations, maximizing the radiative recombination of strain-localized neutral excitons, and suppressing the background of defect-bound states. In the case of GaSe, the exciton and biexcitons are largely overlapped in the spectra, making it challenging to separate them through optical filters^{11,14}. As the presence of biexcitons reduces the purity of SPEs, suppressing the biexciton emissions is vital for high-quality SPEs. To this end, understanding the origin of the exciton complexes in GaSe is important to identify a strategy for the improvement of the SPEs, although it remains elusive.

In this work, we manipulate many-body interactions of strain-localized exciton complexes in GaSe via electrostatic doping, leading to the control of the brightness, single photon purity, and operating

temperatures of the associated GaSe SPEs. We further evaluate the gate-dependent SPE brightness and purity through photoluminescence (PL) spectroscopy and photon antibunching measurements at 4.5K. We find the maximum emission intensity and optimal single photon purity are realized at the charge neutrality point (CNP). Moreover, we show that gating strain-localized SPEs to the CNP maximizes the brightness by suppressing exciton-exciton annihilation (EEA) and minimizing the number of biexcitons, further improving the single photon purity. Temperature-dependent PL and antibunching measurements show the SPEs survive at a higher temperature of 85 K at the CNP, compared to the 23 K without electrostatic doping. We attribute this increased operating temperature to the electrically gated suppression of thermal ionized electrons and biexcitons. The understanding of the combined effects of strain, bias gating, and temperature on exciton complexes and associated SPEs in GaSe provides a crucial foundation for future 2D quantum photonic device applications.

Figure 1a shows the device geometry, where a 50 nm-thick GaSe flake was transferred onto prepatterned electrodes and SiO₂ nanopillar arrays on a Si substrate with 285-nm-thick oxide layer through a dry-release method¹⁵. The pre-patterned electrodes consist of two top electrodes on the oxide layer (labeled as S and D, referring to the source and drain electrodes) and one electrode connecting the back Si as a back gate (labeled as G, referring to the gate electrode). Also, the SiO₂ nanopillar arrays were designed with three diameters of ~ 150 nm, ~ 200 nm, and ~ 250 nm, located between S and D electrodes, and deposited onto the substrate with a height of ~ 130 nm by electron beam deposition. Then the GaSe flake forms a tented structure as reported in our previous work^{11,12}; both ends of the GaSe flake are connected with the electrodes S and D, respectively. Such a design allows both functions of parallel capacitor and field-effect transistor (FET) for 2D materials under strain¹⁶. Moreover, to apply biased gate voltages to the GaSe flake, only the electrodes S and G

are connected to form a parallel capacitor-like device. A detailed description of the substrate design, patterning, and fabrication is in Figure S1 and the methods section. Figure 1b shows an ungated PL spectrum collected from a tented GaSe flake with an incident laser power density of 40 $\text{nW}/\mu m^2$ at 4.5 K. An intense narrow emission line is observed at 1.837 eV (675 nm) which is attribute to strain-localized excitons^{11,12}. In addition, there are multiple emission lines around 1.9 eV that might originate from other localized states. However, we only focus on the emission from exciton complexes that are related to single photon emitters. The photon antibunching of the 1.837 eV (675 nm) exciton emission is characterized via Hanbury Brown-Twiss (HBT) interferometry with a 678 nm narrow bandpass filter. Figure 1c illustrates the measured photon antibunching with a fitted $g^{(2)}(0)$ value of 0.55 \pm 0.06 and a decay time of 3.4 ns. Figure 1d presents the contour map of the PL spectra of the 1.837 eV emitter under gate voltages of +10 V to -15V. Additional PL and photon antibunching results under different gate voltages are shown in Figure S2 in the Supplementary Information. Specifically, at a gate voltage of -7 V, the measured single photon purity $g^{(2)}(0)$ value is minimized to 0.28 \pm 0.03 and the decay time is minimized to 2.8 ns.

The GaSe crystal exhibits n-type characteristics according to the electrical transport measurements shown in Figure S1c. Under negative bias voltage, GaSe will reach a CNP where the radiative recombination of excitons will dominate emission, leading to increased SPE brightness and purity. As shown in Figure 1e, the emission reaches maximum at -7 V gate voltage, indicating that it is close to a CNP. Increasing and decreasing the gate voltage from the CNP results in increased doping by holes and electrons, respectively. The right panel of Figure 1e provides a qualitative energy diagram showing the Fermi energy shift with changing gate voltage. Specifically, from +10 V to -15 V, the Fermi energy is tuned downwards from the conduction band, resulting in an increasing exciton binding energy and a redshift of the emission energy.

In order to better understand the exciton complex formation and the associated SPE behavior in the presence of excess electrons or holes, we investigated another GaSe SPE at 1.777 eV (698 nm) with an incident laser power density of 40 nW/ μ m². Figure 2a shows selected PL spectra from this SPE under bias voltages of -20 V, -7 V, 0 V, and +5 V. More PL spectra and PL maps of this emitter under different voltages are presented in Figure S3. Overall, at a gate voltage of -7 V, the emission intensity of this 1.777 eV band is maximized and enhanced by about 60% compared to that at zero gate voltage.

This 1.777 eV emission band can be deconvolved into an exciton peak X at \sim 1.778 eV (697 nm) and two biexciton peaks XX_1 and XX_2 at ~1.785 eV (694.6 nm) and ~1.773 eV (699.4 nm), respectively. Note the identifications of exciton and biexcitons^{11,14} are based on the powerdependent intensities shown in Figure S4a, where the exciton emission intensities exhibit a sublinear relationship with a power law exponent of 0.8, and the biexciton emission intensities of XX_1 and XX_2 exhibit a superlinear relationship with power-law exponents of 1.18 and 1.32, respectively. Note that the charge-neutral biexciton XX should have a power law exponent twice of that of the exciton. However, this scaling can change when excessive carriers interact with charge-neutral excitons and lower the radiative recombination efficiency¹⁷. Figure S4b shows that, at the CNP (bias voltage = -7V), XX_1 becomes neligible due to its weak emission intensity; the double logarithmic plot of PL intensity as a function of excitation power for biexcitons XX_2 has an exponent of 1.37, which is close to twice of that (0.75) of exciton X. This could be attributed to the thermal equilibrium between the exciton and biexciton states at the CNP. In addition, we also notice the variation of emission intensities above 1.8 eV (as shown in Figure S5) under different voltages. However, we attribute this emission to different localized states not related to single photon emission that are not the focus of this work.

In addition, unlike the common observation of trions (charged excitons) in TMDC monolayers 16,18,19 , trions in GaSe are not generally observed due to non-radiative decay at low photo-generation rates 11,20 and the formation of biexcitons at high photo-generation rates 11,14 . The XX_1 biexciton is observed on the higher energy side of the exciton X with a negative binding energy of -7 meV, due to exciton-exciton repulsion $^{21-24}$. The XX_2 biexciton is observed on the lower energy side of the exciton X with a positive binding energy of +5 meV, due to attractive exciton-exciton interactions. The formation of biexcitons was attributed to the high exciton densities in this Type-I energy funnel in our previous work 12 .

Interestingly, as shown in **Figures S6** and **S7**, when changing bias voltages from +15 V to -20 V, the emission intensity of XX_2 decreases till its minimum at -7V (CNP), then slightly increases with more negative voltages. Meanwhile, the integrated intensity of XX_1 doesn't exhibit significant change during the gate volatge tuning. In addition, the integrated intensity of XX_2 is generally much more prominent than XX_1 during the gate-dependent PL measurements. Moreover, it has been widely reported that a shelving state between the ground state $|0\rangle$ and the excited state $|1\rangle$ in 2D SPEs can trap electrons and holes,^{25,26} leading to $g^{(2)}(\tau)$ >1 for small $|\tau| > 0$.²⁷ As shown in Figure 2b, we observe $g^{(2)}(\tau)$ >1 for small $|\tau| > 0$ when excessive electrons and holes are present (e.g., at +5V and -20V), suggesting that the two biexciton states XX_1 and XX_2 might contribute to the potential shelving states. In contrast, at the CNP, no contribution from the shelving states is observed, and improved SPE purity is observed.

A detailed analysis of the contribution of the shelving states to the photon-antibunching results is shown in **Section 6** of the Supplementary Information. Figure **S6** also shows that the emission intensity of exciton *X* reaches its maximum at the gate voltage of -7V, suggesting that this is the

CNP of this SPE. Meanwhile, the total emission intensities of biexcitons XX_1 and XX_2 are minimized at this gate voltage. Figure 2c shows the ratio of the exciton X emission intensity to the sum of X, XX_1 and XX_2 intensities (defined as the fraction of X) as a function of gate voltage. It clearly shows that the ratio is maximized at the CNP, suggesting that exciton X dominates the PL emission. This can be explained by the electrical suppression of all non-radiative recombination channels²⁸. Correspondingly, Figure 2d shows a minimum $g^{(2)}(0)$ value of 0.43 ± 0.04 is achieved at CNP.

In the dense exciton systems associated with strained 2D semiconductors^{12,29}, the radiative and nonradiative processes are governed by the interactions between excitons²⁸. For GaSe, elastic²⁰ and inelastic exciton-exciton collisions³¹ in the dense exciton system lead to the radiative emission from the exciton and biexcitons and the non-radiative EEA^{31,32}, respectively. Figure **2e** shows an energy diagram depicting the four possible radiative and non-radiative pathways for this SPE. First, the radiative transition from excited state $|1\rangle$ to ground state $|0\rangle$ corresponds to X exciton emission with energy E_X . $|4\rangle$ is the biexciton state located at $2E_X$. However, due to the non-radiative biexciton EEA^{32–35}, no emission is observed from $|4\rangle$. Moreover, repulsive exciton-exciton interactions increase the energy of the biexciton and form state $|2\rangle$, contributing to the XX_1 emission with energy $E_X + E_{BX_1}$ from state $|2\rangle$ to state $|1\rangle$. Similarly, attractive exciton-exciton interactions lower the energy of the biexciton and form state $|3\rangle$, contributing to the XX_2 emission with energy $E_X - E_{BX_1}$ from state $|3\rangle$ to state $|1\rangle$. Therefore, gating GaSe to the CNP suppresses the formation of XX_1 and XX_2 biexcitons and thus maximizes the radiative X exciton emission. It also enhances the SPE purity by suppressing radiative biexciton emission.

The observed EEA suppression can be understood in the context of the density of states (DOS) for electrons in 2D materials and the van Hove singularities (VHSs) that originate from saddle points in the energy dispersion³³. When the optical transition energy approaches a VHS, weak interactions can become more pronounced due to the increased DOS³⁴. In such cases, the enhanced DOS can significantly influence the behavior of electrons and their interactions within the 2D crystal. Specifically, EEA is enhanced when there is a VHS at twice the exciton transition energy³⁵. Indeed, our density functional theory (DFT) simulations (**Figure S8a**) of the joint density of states (JDOS) of unstrained GaSe show a VHS point at an energy twice the bandgap, suggesting EEA contributes to non-radiative processes in unstrained GaSe. Under 1% biaxial tensile strain (**Figure S8b**), the redshift of the exciton transition energy E_X provides sufficient detuning so that $2E_X$ does not overlap with the VHS, resulting in the suppression of EEA and thus enhancement of the exciton emission.

Many excitonic SPEs require low temperature at near 4 K to operate because of unwanted radiative and non-radiative transitions that emerge at higher temperatures ^{13,36,37}, though gate tuning has recently been used to minimize these effects and increase the operation temperature in WSe₂¹³. Here, as shown in Figure 3a, we compare the temperature-dependent photophysics of a 1.827 eV (678.7 nm) GaSe SPE without and with gating to the CNP (Vg= -10 V). More voltage-dependent PL and photon antibunching measurement results of this SPE are shown in **Figure S9** of the Supplementary Information. At 4.5 K, a bias voltage of -10 V leads to a 150 meV redshift of the 1.827 eV (678.7 nm) GaSe SPE to 1.811 eV (684.5 nm), the suppression of biexciton features, and ~30% enhancement of emission intensity. The enhanced SPE brightness and purity at the CNP compared with the ungated emitter are increasingly apparent with increasing temperature. The antibunching results in Figure **3b** (measured with a 683 nm bandpass filter with FWHM = 10 nm

as illustrated in the first PL spectrum of Figure 3a) show that $g^{(2)}(0)$ remains below 0.5 for temperatures up to 85 K when gated to the CNP, while the $g^{(2)}(0)$ increases above 0.5 at T>23 K for the ungated emitter.

The Schön–Klasens mechanism can explain the electrostatic doping-mitigated thermal quenching observed at 65 K^{38–40}. The increasing thermal ionization of acceptors or donors at increasing temperatures results in an enhancement of the non-radiative decay paths discussed in previous sections; the bias voltage at the CNP counter-dopes the n-type GaSe system with holes to suppress the non-radiative decay, resulting in an increase in the quenching temperature.

With a bias voltage of -10 V (CNP) and an incident power density of 13 nW/ μm^2 , the 1.827 eV (678.7 nm) emission band completely quenches above 65 K. However, it can be recovered at higher temperatures with a larger incident power density (as shown in **Figure S10**) because the photogeneration rate modulated by the incident power density determines the formation of exciton complexes and recombination pathways²⁸. As shown in Figure **4a**, the exciton emission peak is recovered with $g^{(2)}(0) = 0.36 \pm 0.04$ at 85 K when tuned to the CNP of -10 V, with an incident power density of 1.4 μ W/ μ m². At 105 K, a reduced exciton emission is observed with the same incident power density (1.4 μ W/ μ m²) and a shelving state emerges with $g^{(2)}(0) = 0.67 \pm 0.07$. At 125 K, a higher incident power density of 10 μ W/ μ m² is applied to recover the exciton luminescence that was completely quenched at 1.4 μ W/ μ m². However, the biexciton feature is very pronounced under such high incident power density, and photon bunching with $g^{(2)}(0) > 1$ is observed, which is a typical chaotic light generated by exciton complexes.^{41,42}

In conclusion, we demonstrate a substantial control of excitonic complexes and the associated SPEs in GaSe using a combination of strain and electrostatic doping. By tuning GaSe to the CNP

with gate voltage, the biexciton population and EEA processes are suppressed. Consequently, the GaSe excitonic SPE brightness is enhanced by ~60%. Moreover, the single photon value g⁽²⁾(0) is reduced from 0.55 to 0.28 at the CNP, and the maximum operating temperature is enhanced from 23 K at zero bias voltage to 85 K at a gate voltage of -10V. The comprehensive understanding of the combined effect of nanoscale strain and electrostatic doping on 2D SPEs provides a foundation for the design of bright GaSe SPEs with high single photon purity operating at higher temperatures. More broadly, these results enable new approaches for 2D quantum photonic devices and photonic quantum information technology and for fundamental studies of strong Coulomb interactions in many-body systems.

Methods. Synthesis of bulk GaSe crystal. Bulk GaSe was synthesized by the chemical vapor transport (CVT) method.⁴³ The details of the recipe can be found in our previous report.¹¹

Fabrication of electrical device with SiO₂ nanopillar arrays and the transport measurement. The device fabrication is described in Section 1 of the Supplementary Information. The transport measurements were carried out at 77 K via a CIA RC102-CFM microscopy cryostat with electrical feed-throughs. The electrical control was performed by two Keithley 2400 source meters that were controlled by our Matlab codes. The evaluation of the actual electrical field is discussed in detail in Section 9 of the Supplementary Information.

Transfer of GaSe flake SiO₂ nanopillar arrays. The GaSe flakes were exfoliated onto a blank Si chip with a 285-nm-thick oxide layer, then a thin layer of poly-propylene carbonate (PPC) was spin-coated onto the chip at 2,000 rpm/min for 45s. After curing at 60 °C for 5 mins, the PPC layer carrying the GaSe flakes was detached from the chip and transferred onto the SiO₂ nanopillar arrays under the microscope.

Optical spectroscopy. The cryo-PL and associated photon statistics measurements were performed in a home-built confocal PL microscope in a backscattering configuration. A Princeton Instruments Isoplane SCT-320 spectrograph with a Pixis 400BR Excelon camera and a grating turret with 150 g/mm, 600 g/mm, and 2400 g/mm gratings were used to measure PL spectra with spectral resolutions of ~ 3.25 meV, $\sim 300~\mu$ eV, and $\sim 30~\mu$ eV, respectively. A 532 nm diode laser (Cobolt) was used for excitation. A 100x in-vacuum objective (Zeiss, NA = 0.85) was integrated with the Montana S100 closed-cycle cryostat, resulting in a spatial resolution of ~ 500 nm. The PL mapping was controlled by 2-axis galvo scanning. The photon-antibunching measurements utilized a pair of large-area superconducting nanowire single-photon detectors (SNSPDs, Quantum Opus) and a

Swabian Time Tagger 20 time-correlated single photon counting (TCSPC) system. A 90:10 non-

polarizing beam splitter was used to allow for PL (10% coupling efficiency) and photon correlation

functions (90% coupling efficiency) to be acquired in parallel.

DFT simulations. Plane-wave DFT calculations were carried out using the Vienna Ab initio

Simulation Package^{28,29} (VASP) with projector augmented wave (PAW) pseudopotentials^{28,30,31}

for electron-ion interactions, and the generalized gradient approximation (GGA) functional of

Perdew, Burke and Ernzerhof⁴⁴ (PBE) for exchange-correlation interactions. The details of

geometry optimization could be referred to our previous work¹¹. The analysis of the total density

of states was carried out using the VASPKIT package⁴⁵.

AUTHOR INFORMATION

Corresponding Author

*Email: xiling@bu.edu; puretzkya@ornl.gov; lawriebj@ornl.gov

The authors declare no competing financial interest.

ACKNOWLEDGEMENTS

This material is based upon work supported by the National Science Foundation (NSF) under

Grant No. (1945364). Work by X.L. was supported by the U.S. Department of Energy (DOE),

Office of Science, Basic Energy Sciences (BES) under Award DE-SC0021064. W.L., X.L. and

A.K.S acknowledge the support of National Science Foundation (NSF) under Grant No.

(2111160). The photoluminescence and photon statistics measurements were performed at the

Center for Nanophase Materials Sciences (CNMS), which is a US Department of Energy Office

of Science User Facility. W.L. acknowledges Dr. Y.Y. Pai from Oak Ridge National Laboratory

13

for his help with experimental automation. X.L. and A.K.S. acknowledge the membership of the Photonics Center at Boston University. The computational work is performed using Shared Computing Cluster (BUSCC) at Boston University.

AUTHOR CONTRIBUTIONS

W.L. and X.L. conceived the experiment. W.L. prepared samples with assistance from Q.T. and H.G. Q.T. and H.G. synthesized and characterized the bulk GaSe crystals. W.L. conducted the PL and photon-statistics measurements with assistance from A.P. and B.L at the Center for Nanophase Materials Sciences, Oak Ridge National Laboratory. W.L performed theoretical calculations with assistance from L.L. W.L performed the analysis and interpretation of the data with assistance from A.P., B.L., L.L., A.K.S. and X.L. All authors contributed to the writing of the manuscript.

ASSOCIATED CONTENTS

Supporting information

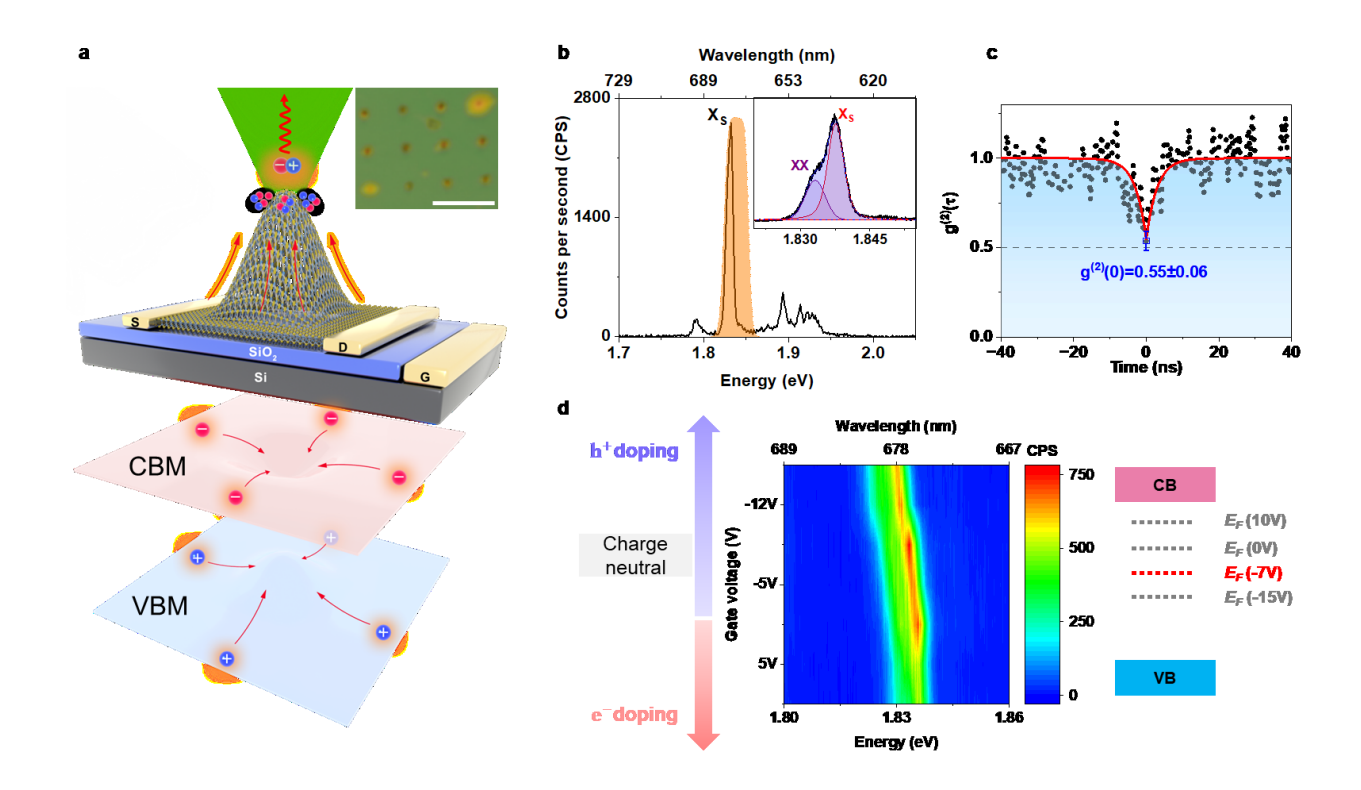
The Supporting Information is available free of charge at XXX. Description of sample preparation methods; PL mapping and photon antibunching results of the 1.837 eV (675 nm) GaSe SPE; PL spectra and mapping results of the 1.777 eV (698 nm) GaSe SPE; Summary of the emission intensities of the 1.777 eV (698 nm) GaSe SPE; Density functional theory (DFT) simulations result of the joint density of states (JDOS); PL and photon antibunching results of the 1.827 eV (678.7 nm) GaSe SPE; SNSPD intensity counts of the 1.827 eV (678.7 nm) GaSe SPE at 65 K, 85 K and 105 K; and evaluation of electric field (PDF).

REFERENCES

- (1) Couteau, C.; Barz, S.; Durt, T.; Gerrits, T.; Huwer, J.; Prevedel, R.; Rarity, J.; Shields, A.; Weihs, G. Applications of Single Photons to Quantum Communication and Computing. *Nat. Rev. Phys.* **2023**, *5*, 326–338. https://doi.org/10.1038/s42254-023-00583-2.
- (2) Gyger, S.; Zichi, J.; Schweickert, L.; Elshaari, A. W.; Steinhauer, S.; Covre da Silva, S. F.; Rastelli, A.; Zwiller, V.; Jöns, K. D.; Errando-Herranz, C. Reconfigurable Photonics with On-Chip Single-Photon Detectors. *Nat. Commun.* **2021**, *12* (1), 1408.
- (3) Vaidya, S.; Gao, X.; Dikshit, S.; Aharonovich, I.; Li, T. Quantum Sensing and Imaging with Spin Defects in Hexagonal Boron Nitride. *Adv. Phys. X* **2023**, *8* (1), 2206049.
- (4) Aharonovich, I.; Englund, D.; Toth, M. Solid-State Single-Photon Emitters. *Nat. Photonics* **2016**, *10* (10), 631–641. https://doi.org/10.1038/nphoton.2016.186.
- (5) Caldwell, J. D.; Aharonovich, I.; Cassabois, G.; Edgar, J. H.; Gil, B.; Basov, D. N. Photonics with Hexagonal Boron Nitride. *Nat. Rev. Mater.* **2019**, *4* (8), 552–567. https://doi.org/10.1038/s41578-019-0124-1.
- (6) Mendelson, N.; Chugh, D.; Reimers, J. R.; Cheng, T. S.; Gottscholl, A.; Long, H.; Mellor, C. J.; Zettl, A.; Dyakonov, V.; Beton, P. H. Identifying Carbon as the Source of Visible Single-Photon Emission from Hexagonal Boron Nitride. *Nat. Mater.* 2021, 20 (3), 321–328.
- (7) White, S. J.; Yang, T.; Dontschuk, N.; Stewart, C.; Li, C.; Xu, Z.-Q.; Solntstev, A. S.; Kianinia, M.; Stacey, A.; Toth, M. Hexagonal Boron Nitride: A Source for Quantum Photonics Applications. In *Light-Emitting Devices, Materials, and Applications XXVII*; SPIE, 2023; Vol. 12441, pp 59–62.
- (8) Turunen, M.; Brotons-Gisbert, M.; Dai, Y.; Wang, Y.; Scerri, E.; Bonato, C.; Jöns, K. D.; Sun, Z.; Gerardot, B. D. Quantum Photonics with Layered 2D Materials. *Nat. Rev. Phys.* **2022**, *4* (4), 219–236.
- (9) Gao, T.; von Helversen, M.; Anton-Solanas, C.; Schneider, C.; Heindel, T. Atomically-Thin Single-Photon Sources for Quantum Communication. *Npj 2D Mater. Appl.* **2023**, 7 (1), 4.
- (10) Gupta, S.; Wu, W.; Huang, S.; Yakobson, B. I. Single-Photon Emission from Two-Dimensional Materials, to a Brighter Future. J. Phys. Chem. Lett. 2023, 14 (13), 3274–3284.
- (11) Luo, W.; Puretzky, A. A.; Lawrie, B. J.; Tan, Q.; Gao, H.; Chen, Z.; Sergienko, A. V.; Swan, A. K.; Liang, L.; Ling, X. Deterministic Localization of Strain-Induced Single-Photon Emitters in Multilayer GaSe. *ACS Photonics* **2023**, *10* (8), 2530–2539. https://doi.org/10.1021/acsphotonics.3c00052.
- (12) Luo, W.; Lawrie, B.; Puretzky, A.; Tan, Q.; Eichman, G.; Mcgee, E.; Swan, A.; Liang, L.; Ling, X. Imaging Strain-Localized Single-Photon Emitters in Layered GaSe below the Diffraction Limit. arXiv:2305.03230 (physics.optics). 2023, https://doi.org/10.48550/arXiv.2305.03230.
- (13) Stevens, C. E.; Chuang, H.-J.; Rosenberger, M. R.; McCreary, K. M.; Dass, C. K.; Jonker, B. T.; Hendrickson, J. R. Enhancing the Purity of Deterministically Placed Quantum Emitters in Monolayer WSe2. *ACS Nano* **2022**, *16* (12), 20956–20963.
- (14) Tonndorf, P.; Schwarz, S.; Kern, J.; Niehues, I.; Del Pozo-Zamudio, O.; Dmitriev, A. I.; Bakhtinov, A. P.; Borisenko, D. N.; Kolesnikov, N. N.; Tartakovskii, A. I. Single-Photon Emitters in GaSe. *2D Mater.* **2017**, *4* (2), 021010.
- (15) Kinoshita, K.; Moriya, R.; Onodera, M.; Wakafuji, Y.; Masubuchi, S.; Watanabe, K.; Taniguchi, T.; Machida, T. Dry Release Transfer of Graphene and Few-Layer h-BN by Utilizing Thermoplasticity of Polypropylene Carbonate. *Npj 2D Mater. Appl.* **2019**, *3* (1), 22.

- (16) Chen, Z.; Luo, W.; Liang, L.; Ling, X.; Swan, A. K. Charge Separation in Monolayer WSe2 by Strain Engineering: Implications for Strain-Induced Diode Action. *ACS Appl. Nano Mater.* **2022**, *5* (10), 15095–15101.
- (17) Barbone, M.; Montblanch, A. R.-P.; Kara, D. M.; Palacios-Berraquero, C.; Cadore, A. R.; De Fazio, D.; Pingault, B.; Mostaani, E.; Li, H.; Chen, B. Charge-Tuneable Biexciton Complexes in Monolayer WSe2. *Nat. Commun.* **2018**, *9* (1), 3721.
- (18) Mak, K. F.; He, K.; Lee, C.; Lee, G. H.; Hone, J.; Heinz, T. F.; Shan, J. Tightly Bound Trions in Monolayer MoS2. *Nat. Mater.* **2013**, *12* (3), 207–211.
- (19) Kesarwani, R.; Simbulan, K. B.; Huang, T.-D.; Chiang, Y.-F.; Yeh, N.-C.; Lan, Y.-W.; Lu, T.-H. Control of Trion-to-Exciton Conversion in Monolayer WS2 by Orbital Angular Momentum of Light. *Sci. Adv.* **2022**, *8* (13), eabm0100.
- (20) Del Pozo-Zamudio, O.; Schwarz, S.; Sich, M.; Akimov, I. A.; Bayer, M.; Schofield, R. C.; Chekhovich, E. A.; Robinson, B. J.; Kay, N. D.; Kolosov, O. V. Photoluminescence of Two-Dimensional GaTe and GaSe Films. *2D Mater.* **2015**, *2* (3), 035010.
- (21) Rodt, S.; Heitz, R.; Schliwa, A.; Sellin, R. L.; Guffarth, F.; Bimberg, D. Repulsive Exciton-Exciton Interaction in Quantum Dots. *Phys. Rev. B* **2003**, *68* (3), 035331.
- (22) Stier, O. Theory of the Electronic and Optical Properties of Ingaas/Gaas Quantum Dots. In *Nano-Optoelectronics*; Springer, 2002; pp 167–202.
- (23) Stier, O.; Schliwa, A.; Heitz, R.; Grundmann, M.; Bimberg, D. Stability of Biexcitons in Pyramidal Inas/Gaas Quantum Dots. *Phys. Status Solidi B* **2001**, *224* (1), 115–118.
- (24) Lelong, P.; Heller, O.; Bastard, G. Coulomb Interactions in Small InAs Quantum Dots. *Solid-State Electron.* **1998**, *42* (7–8), 1251–1256.
- (25) Boll, M. K.; Radko, I. P.; Huck, A.; Andersen, U. L. Photophysics of Quantum Emitters in Hexagonal Boron-Nitride Nano-Flakes. *Opt. Express* **2020**, *28* (5), 7475–7487.
- (26) Feldman, M. A.; Marvinney, C. E.; Puretzky, A. A.; Lawrie, B. J. Evidence of Photochromism in a Hexagonal Boron Nitride Single-Photon Emitter. *Optica* **2021**, 8 (1), 1–5.
- (27) Berthel, M.; Mollet, O.; Dantelle, G.; Gacoin, T.; Huant, S.; Drezet, A. Photophysics of Single Nitrogen-Vacancy Centers in Diamond Nanocrystals. *Phys. Rev. B* **2015**, *91* (3), 035308.
- (28) Lien, D.-H.; Uddin, S. Z.; Yeh, M.; Amani, M.; Kim, H.; Ager, J. W.; Yablonovitch, E.; Javey, A. Electrical Suppression of All Nonradiative Recombination Pathways in Monolayer Semiconductors. *Science* **2019**, *364* (6439), 468–471.
- (29) Branny, A.; Kumar, S.; Proux, R.; Gerardot, B. D. Deterministic Strain-Induced Arrays of Quantum Emitters in a Two-Dimensional Semiconductor. *Nat. Commun.* **2017**, *8* (1), 15053. https://doi.org/10.1038/ncomms15053.
- (30) Ugumori, T.; Masuda, K.; Namba, S. Exciton Absorption in GaSe under Intense Excitation. J. Phys. Soc. Jpn. 1977, 43 (1), 151–156.
- (31) Mercier, A.; Voitchovsky, J. P. Exciton-Exciton and Exciton-Carrier Scattering in GaSe. *Phys. Rev. B* **1975**, *11* (6), 2243.
- (32) Capozzi, V.; Staehli, J. L. Spontaneous and Optically Amplified Luminescence from Exciton-Exciton Collisions in GaSe at Liquid-He Temperature. *Phys. Rev. B* **1983**, *28* (8), 4461.
- (33) Van Hove, L. The Occurrence of Singularities in the Elastic Frequency Distribution of a Crystal. *Phys. Rev.* **1953**, *89* (6), 1189.

- (34) Hirsch, J. E.; Scalapino, D. J. Enhanced Superconductivity in Quasi Two-Dimensional Systems. *Phys. Rev. Lett.* **1986**, *56* (25), 2732.
- (35) Kim, H.; Uddin, S. Z.; Higashitarumizu, N.; Rabani, E.; Javey, A. Inhibited Nonradiative Decay at All Exciton Densities in Monolayer Semiconductors. *Science* **2021**, *373* (6553), 448–452.
- (36) Luo, Y.; Liu, N.; Li, X.; Hone, J. C.; Strauf, S. Single Photon Emission in WSe 2 up 160 K by Quantum Yield Control. *2D Mater.* **2019**, *6* (3), 035017. https://doi.org/10.1088/2053-1583/ab15fe.
- (37) Parto, K.; Azzam, S. I.; Banerjee, K.; Moody, G. Defect and Strain Engineering of Monolayer WSe2 Enables Site-Controlled Single-Photon Emission up to 150 K. *Nat. Commun.* **2021**, *12* (1), 1–8.
- (38) Schön, M. Zum Leuchtmechanismus Der Kristallphosphore. Z. Für Phys. **1942**, 119 (7–8), 463–471.
- (39) Klasens, H. A. Transfer of Energy between Centres in Zinc Sulphide Phosphors. *Nature* **1946**, *158* (4009), 306–307.
- (40) Reshchikov, M. A. Mechanisms of Thermal Quenching of Defect-Related Luminescence in Semiconductors. *Phys. Status Solidi A* **2021**, *218* (1), 2000101.
- (41) Kuroda, T.; Belhadj, T.; Abbarchi, M.; Mastrandrea, C.; Gurioli, M.; Mano, T.; Ikeda, N.; Sugimoto, Y.; Asakawa, K.; Koguchi, N. Bunching Visibility for Correlated Photons from Single GaAs Quantum Dots. *Phys. Rev. B* **2009**, *79* (3), 035330.
- (42) Wang, Z.; Rasmita, A.; Long, G.; Chen, D.; Zhang, C.; Garcia, O. G.; Cai, H.; Xiong, Q.; Gao, W. Optically Driven Giant Superbunching from a Single Perovskite Quantum Dot. *Adv. Opt. Mater.* **2021**, *9* (21), 2100879.
- (43) Ishii, T.; Kambe, N. GaSe Single Crystal Growth by Iodine Vapor Transport. *J. Cryst. Growth* **1986**, 76 (2), 489–493.
- (44) Perdew, J. P.; Burke, K.; Ernzerhof, M. Generalized Gradient Approximation Made Simple. *Phys. Rev. Lett.* **1996**, *77* (18), 3865.
- (45) Wang, V.; Xu, N.; Liu, J.-C.; Tang, G.; Geng, W.-T. VASPKIT: A User-Friendly Interface Facilitating High-Throughput Computing and Analysis Using VASP Code. *Comput. Phys. Commun.* **2021**, *267*, 108033.



scale is 5 μ m. (b) PL spectrum of an SPE at ~ 1.837 eV (~ 675 nm) excited by a 532 nm continuous wave (cw) laser with an incident laser power density of 40 nW/ μ m² at 4.5 K. The spectrum is acquired with a 150-grooves/mm grating (spectral resolution ~ 1 meV). The shaded area highlights the spectral range of a 678 nm bandpass filter (FWHM = 10 nm) used for the following photon-antibunching measurements. The inset is a corresponding PL spectrum collected with 600 grooves/mm grating (spectral resolution ~ 0.25 meV) that can be deconvoluted into excitonic, X_S ,

and biexcitonic, XX spectral lines. (c) Second order autocorrelation function, g⁽²⁾(t), acquired

without biasing using a narrow bandpass filter centered at 678 nm with full width at half maximum

(FWHM) of 10 nm. The fitted $g^{(2)}(0) = 0.48 \pm 0.05$. (d) Contour map of the PL spectra of the 1.837

eV (675 nm) SPE measured at T = 4.5 K under bias-gating and with a 600 grooves/mm grating.

The left panel suggests that negative gate voltages introduce holes into the material; while the

Figure 1. Electrical gating of SPEs in nano-pillar strained GaSe. (a) Illustration of the device.

The inset shows an optical image of a ~50-nm-thick GaSe flake on SiO₂ nanopillar arrays, and the

positive gate voltages would result in electron doping; the charge neutral point is around -7V for this emitter. The right energy level diagram depicts the position of Fermi level with different voltages.

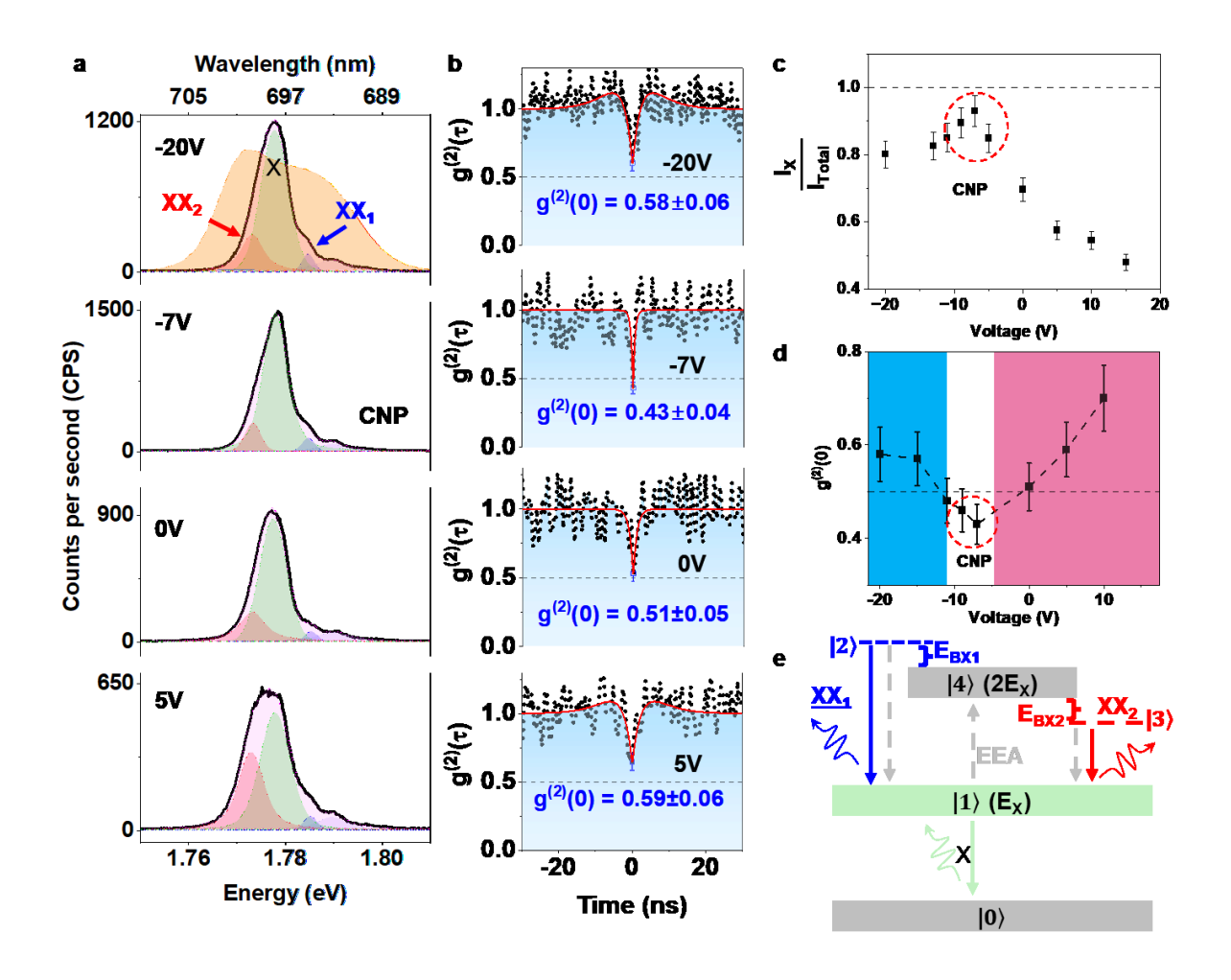


Figure 2. Gate tuning of a 698 nm SPE at T = 4.5 K with an incident laser power density of $40 \text{ nW}/\mu m^2$. (a) Typical PL spectra acquired with bias-gate voltages of -20 V, -7 V, 0 V and 5 V, respectively. The fits to an exciton peak at ~1.778 eV (~ 697 nm) and two biexciton peaks XX_1 and XX_2 at ~1.785 eV (~ 694.6 nm) and ~1.773 eV (~ 699.4 nm), respectively are shown. A 700 nm bandpass filter (FWHM = 10 nm) was used for the photon antibunching measurements on this SPE, The measured response of the bandpass filter used for antibunching measurements is highlighted in the -20 V spectrum with orange shade. (b) Photon antibunching measured for this 698 nm emitter with bias-gate voltages of -20 V, -7 V, 0 V, and 5 V, respectively. (c) Ratio of the

exciton PL intensity to the integrated exciton and biexciton intensity $(\frac{I_X}{I_{Total}})$ as a function of the gate voltage. (d) $g^{(2)}(0)$ values as a function of the gate voltage. (e) Energy diagram of four possible electronic transition pathways of this 698 nm emitter, the red, green, and blue arrows suggest the radiative decay pathways, while the gray dashed arrows suggest the non-radiative decay pathways.

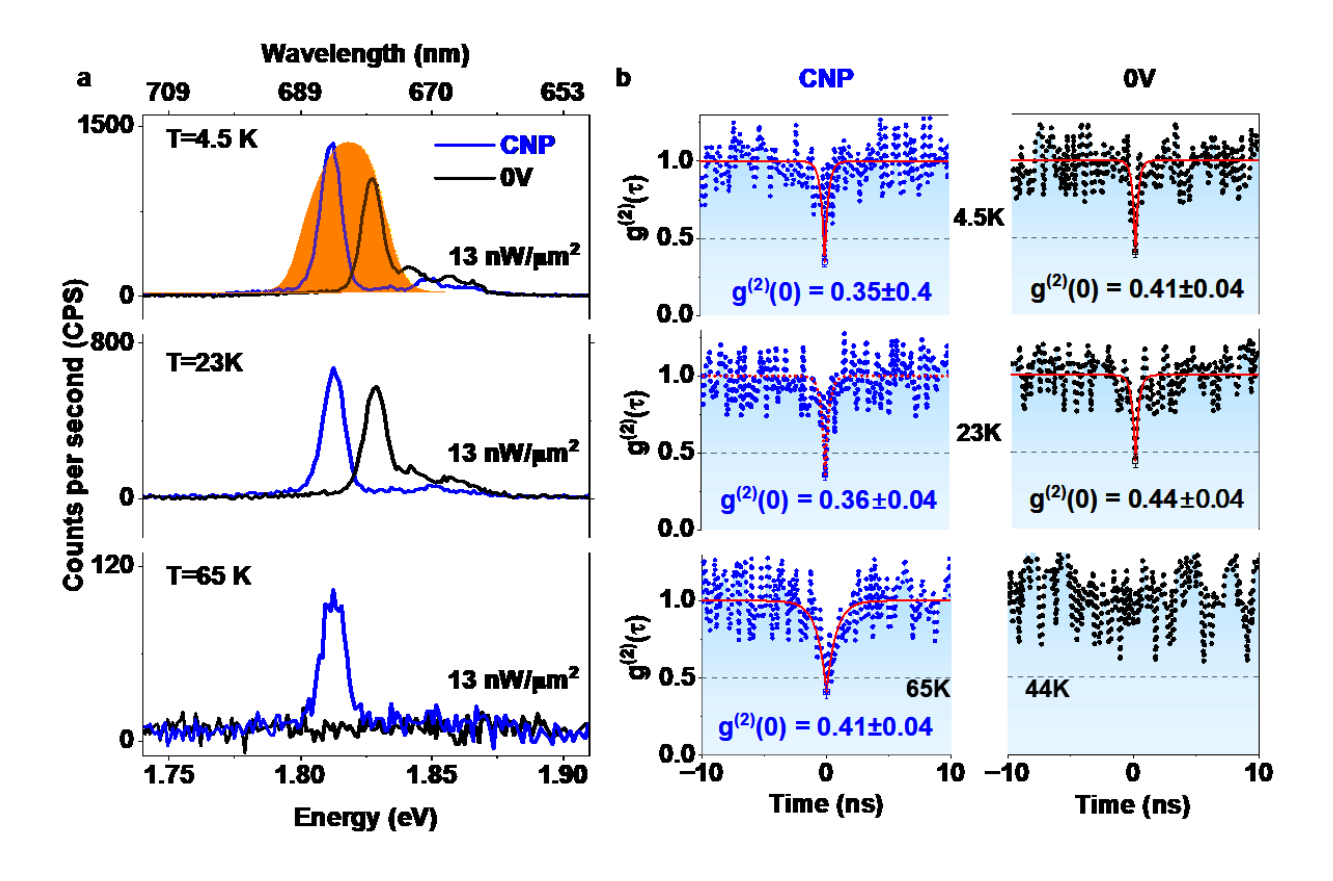


Figure 3. Temperature-dependent PL and antibunching measurements of a 1.827 eV (678.7 nm) GaSe SPE without and with gating to the CNP point (V_g =-10 V) with an incident laser power density of 13 nW/ μ m². (a) PL spectra of this 678.7 nm SPE at 4.5 K, 23 K and 65 K, respectively. At T = 65 K, the PL of the unbiased emitter quenches. (b) Photon-antibunching measured for this 678.7 nm emitter with a bandpass filter (683 nm, FWHM = 10 nm, measured filter bandwidth highlighted in the shaded area). When gated to the CNP, reasonable antibunching remains at temperatures up to 65 K; when ungated, reasonable antibunching remains at temperatures up to 23 K.

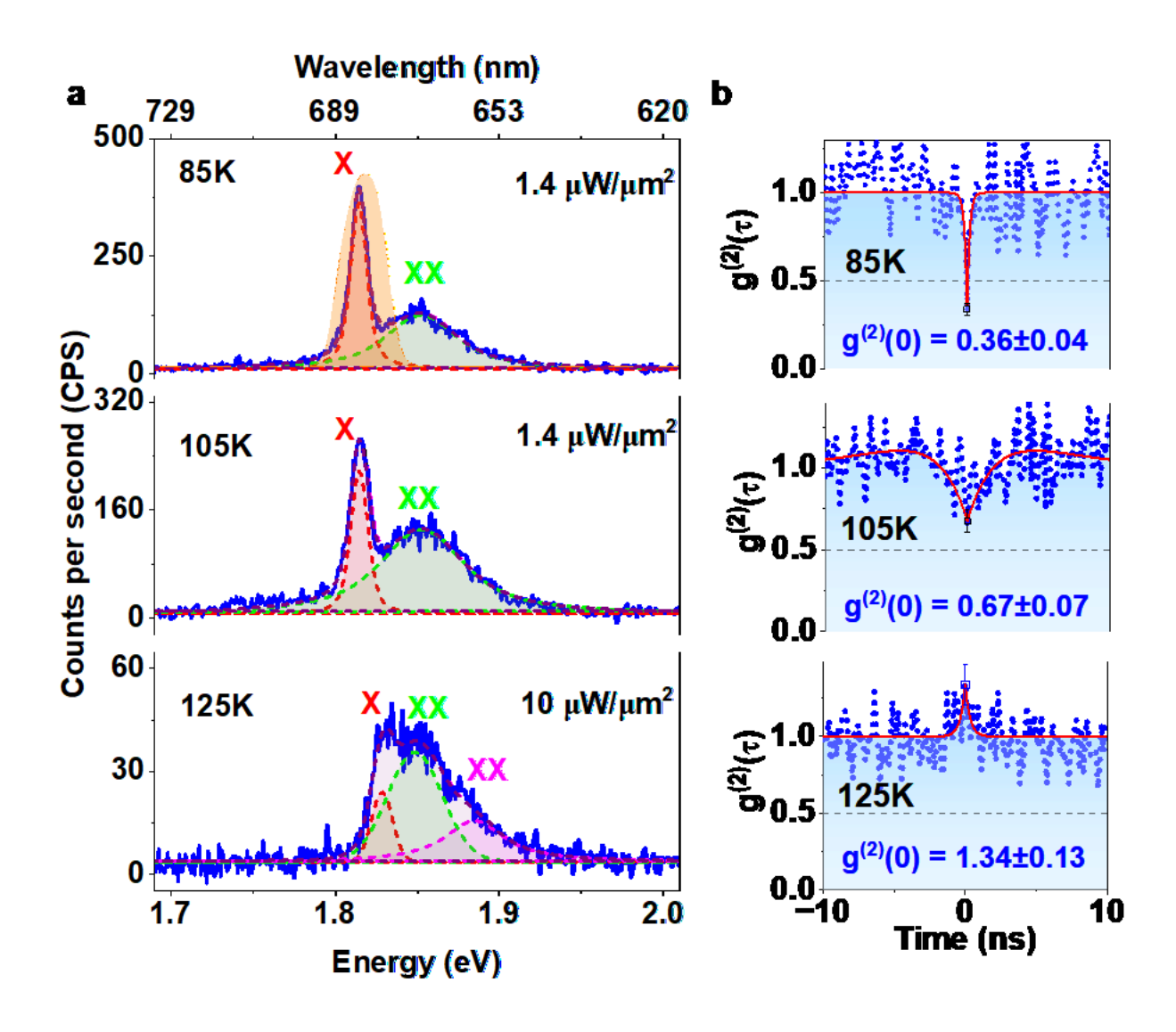


Figure 4. Degradation of photon antibunching with increasing temperature of the 678.7 nm SPE under its CNP point (V_g =-10 V). (a) PL spectra measured for this 678.7 nm emitter at 85, 105, and 125 K. The incident power densities are 1.4 $\mu W/\mu m^2$ at 85 K and 105 K, and 10 $\mu W/\mu m^2$ at 125 K. (b) The measured $g^2(\tau)$ of this 678.7 nm SPE acquired with a narrow bandpass filter (683 nm, FWHM = 10 nm; as highlighted in the top spectrum of (a) by the orange shade).

ToC

